Modulation of Magnetic Properties in $Ni_{0.4}Zn_{0.6}Fe_2O_4$ Spinel Ferrite by Additives

Kwang-Rok Mun and Young-Min Kang*

*Department of Materials Science and Engineering, Korea National University of Transportation,
Chungju 27469, Republic of Korea*

Sintered $Ni_{0.4}Zn_{0.6}Fe_2O_4$ ferrite with various additives, namely, CoO, Cu_2O, SiO_2, $CaCO_3$, and MgO was prepared by conventional ceramic processes. The formation of a single-phase cubic spinel structure was confirmed by powder X-ray diffraction. The microstructure and magnetic properties of the samples were significantly changed by the type of additive. In the frequency-dependent complex permeability (μ', μ'') measurement, it was found that Cu_2O and CoO were more effective than the other additives for modulating the μ', μ'' spectra. This was because a larger spectrum shift, either to a lower or higher frequency, could be achieved by the same doping amount of 1 wt.%. When the doping amount of CoO increased up to 3 wt.%, the μ', μ'' spectra gradually shifted to a higher frequency following Snoek's limitation law. The co-doping of 1.5 wt.% CoO and 0.5 wt.% Cu_2O was more effective for radio-frequency identification (RFID) applications than any individual doping because a relatively large real part of the permeability ($\mu' = 125.3$) and small loss factor ($\mu'' = 5.8$) could be achieved simultaneously at the frequency of 13.56 MHz.

Keywords : spinel ferrites, complex permeability, sintering additives

1. Introduction

During the past decades, soft magnetic materials have attracted considerable attention owing to their useful electromagnetic properties and wide range of applications. Among the soft magnetic materials, cubic-structured Ni–Zn spinel ferrites are some of the important material systems used in various electromagnetic devices, such as telecommunication systems, microwave devices, and power transformers, because of their high magnetic permeability with a small magnetic loss and high electrical resistivity [1-3]. Their applications in high-frequency devices can be classified based on the complex relative permeability, $\mu = \mu'$-$j\mu''$. The real part of the complex permeability μ' represents the storage capability of magnetic energy, and the imaginary part μ'' stands for the magnetic energy loss. A high μ' and $\mu'' \approx 0$ are ideal for applications in magnetic field shielding, wireless charging, inductors, and transformers. In addition, a high μ'' is required for the electromagnetic wave absorber employed in the corresponding frequency range.

Ni–Zn ferrites have been prepared by various technologies, such as typical ceramic processes [4, 5], co-precipitation [6, 7], and sol–gel methods [8, 9]. Their magnetic properties strongly depend on the fabrication process and cation composition. It has been reported that cation substitution in spinel ferrites significantly affects their microstructure and magnetic properties [10-14]. In our previous study, the structural and magnetic properties of $Ni_xZn_{1-x}Fe_2O_4$ ($0.2 \leq x \leq 0.8$) ferrites prepared by a solid-state reaction process were investigated [15]. Frequency-dependent complex permeability spectra could be tuned by the Ni substitution amount, x.

Also, employing sintering additives during the ball milling of calcined powder is indispensable for obtaining high density ceramic samples. It is well known that SiO_2 suppresses grain growth and CaO (or $CaCO_3$) promotes densification during sintering process. In case of magnetic spinel ferrites, these additives are effective not only in tailoring a dense microstructure but also in modulating magnetic properties [16]. In the present research, the effect of various sintering additives on the structural and magnetic properties of $Ni_{0.4}Zn_{0.6}Fe_2O_4$ (NZF) ($x = 0.4$) ferrites were systematically investigated.

*Corresponding author: Tel: +82-43-841-5382
Fax: +82-43-841-5380, e-mail: ymkang@ut.ac.kr

2. Experimental Procedure

Stoichiometric NZF was prepared by conventional solid-state reaction processes. The precursor powders of NiO (99.9 %), ZnO (99.9 %), and Fe_2O_3 (99.9 %) were weighed in accordance with the cation ratios in the chemical formulae. The weighed mixtures were ball-milled for 20 h in deionized (DI) water in a polypropylene jar and using zirconia balls and then calcined in an alumina crucible at 1250 °C in air for 4 h. Then the calcined powder samples were ball milled again for 20 h with zirconia balls. After drying the ball-milled powder, the powder samples were pressed in a mold to form a toroidal-shaped green compact with inner/outer diameter of 9 mm/14.8 mm. The palletized samples were sintered in a box furnace at 1250 °C for 2 h. Various additives, as listed in Table 1, were mixed during the second ball-milling process. The sample density was calculated based on the weight and geometric dimensions of the samples. X-ray diffraction (XRD, D8 Advance, Bruker) with a Cu K_α radiation source (λ = 0.154056 nm) was performed for the crystalline phase analysis. Sintered samples were ground to a powder form for the XRD measurement. Microstructural observation of the fractured surface of the sintered samples was conducted via field-emission scanning electron microscopy (FE-SEM, JSM-7610F, JEOL). Initial magnetization and magnetic hysteresis curves (B–H) were measured by using a soft magnetic measurement system (Remagraph C-530, Magnet-Physik). The toroidal sintered samples wound by a typical enameled copper wire were used for the B–H measurement. Complex permeability spectra (1 MHz–1 GHz) of the samples were obtained by using an impedance Analyzer (E4991A, Agilent) equipped with a fixture for magnetic permeability measurement (16454A).

Table 1 lists the sample IDs for the different samples doped with the various selected additives.

3. Results and Discussion

Figure 1 (a) shows the XRD patterns of the sintered
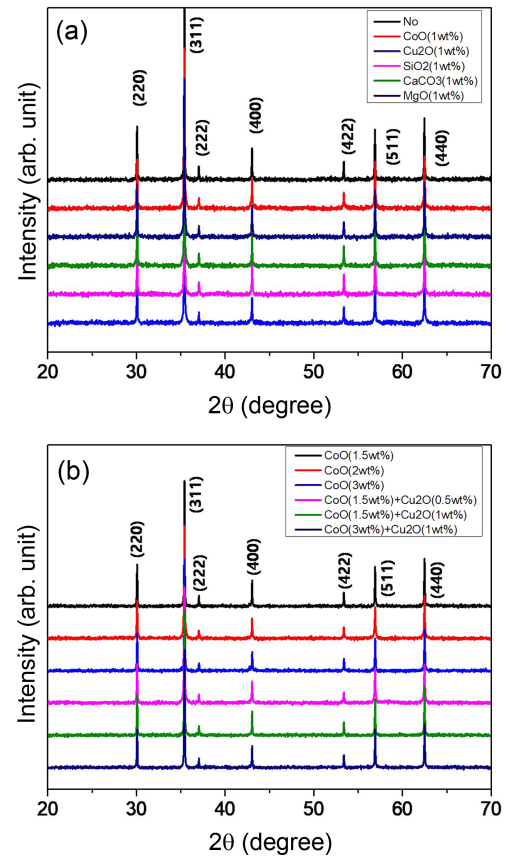
Fig. 1. (Color online) (a) and (b) XRD patterns of $Ni_{0.4}Zn_{0.6}Fe_2O_4$ ferrite with various additives.

Table 1. Sintered density (ρ), average grain size (D_{ave}), magnetic flux density at H = 30 Oe ($B_{H=30Oe}$), coercivity (H_C), real part of the permeability (μ') at 1 MHz, maximum imaginary part of the permeability (μ''_{max}), and frequency at the maximum μ'' ($f_{\mu''max}$).

ID	Additives	ρ (g/cm³)	D_{ave} (μm)	$B_{H=30Oe}$ (G)	H_C (Oe)	μ' (@ 1 MHz)	μ''_{max}	$f_{\mu''\,max}$ (MHz)
NZF0	No	5.26	1.77	3755	0.33	367.7	166.4	8.05
NZF1	CoO (1 wt.%)	5.37	1.74	3409	0.84	168.1	93.7	29.5
NZF2	Cu_2O (1 wt.%)	5.35	2.24	3822	0.26	557.0	248.6	4.12
NZF3	SiO_2 (1 wt.%)	5.33	1.35	3483	1.08	331.6	163.0	11.2
NZF4	$CaCO_3$ (1 wt.%)	5.35	2.06	3691	0.56	441.4	179.4	6.46
NZF5	MgO (1 wt.%)	5.31	1.52	3222	0.55	403.3	186.5	7.67
NZF6	CoO (1.5 wt.%)	5.32	1.79	3753	1.24	114.1	72.0	49.6
NZF7	CoO (2 wt.%)	5.38	1.68	3628	1.81	91.0	67.0	70.0
NZF8	CoO (3 wt.%)	5.31	1.63	3669	2.59	77.5	52.1	86.1
NZF9	CoO (1.5 wt.%), Cu_2O (0.5 wt.%)	5.44	2.31	3827	1.12	113.1	74.4	56.9
NZF10	CoO (1.5 wt.%), Cu_2O (1 wt.%)	5.33	>10	3663	1.35	131.3	78.3	47.9
NZF11	CoO (3 wt.%), Cu_2O (1 wt.%)	5.32	>10	3274	2.90	59.5	38.0	106.0
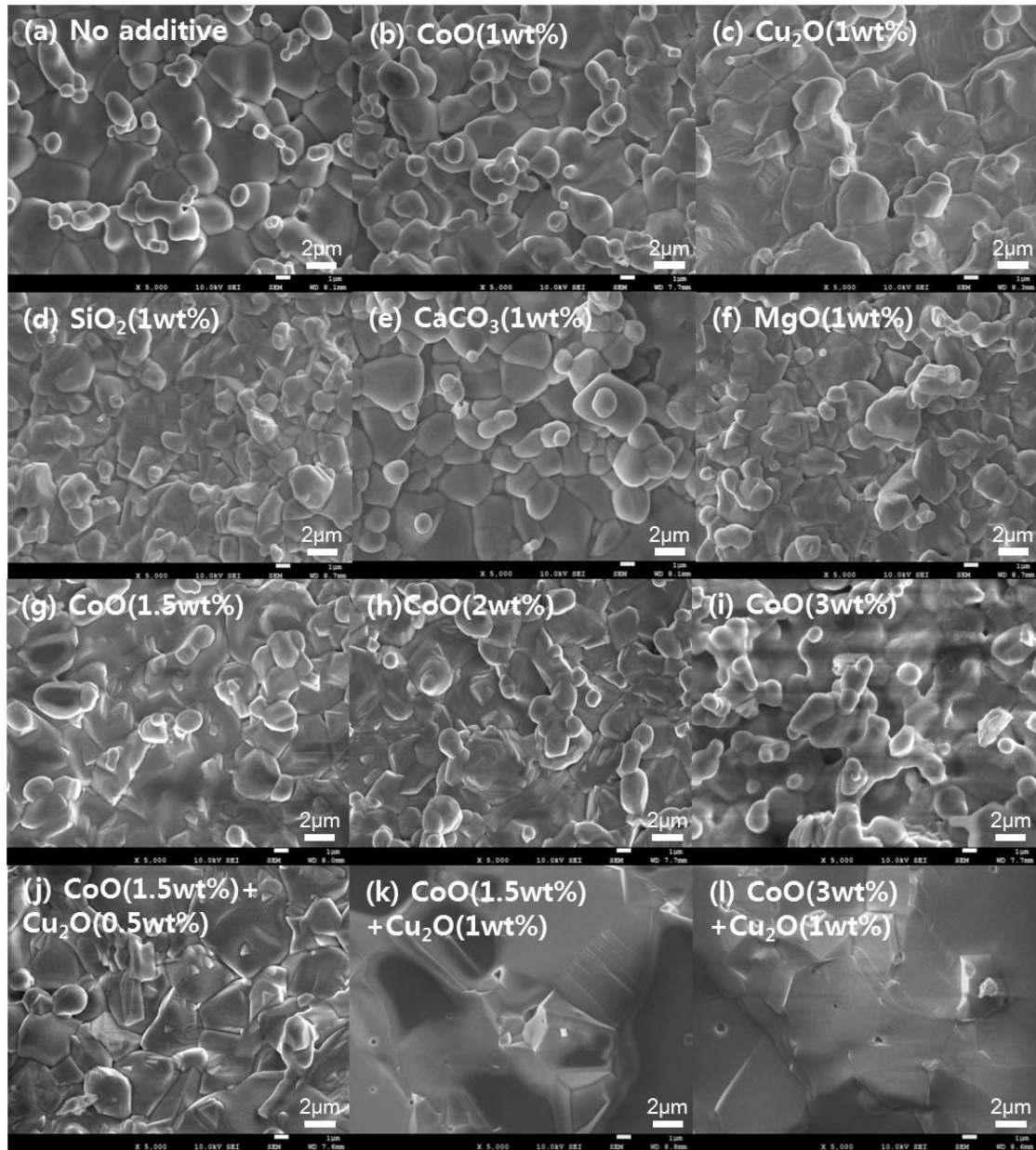
Fig. 2. SEM micrographs of $Ni_{0.4}Zn_{0.6}Fe_2O_4$ ferrite with various additives.

NZF samples doped with the various selected additives: CoO, Cu_2O, SiO_2, $CaCO_3$, and MgO (all 1 wt.%). The pattern of NZF without any additive (NZF0) is also presented as the top line in Fig. 1(a). All the sintered samples show patterns of a single spinel phase. The patterns of the NZF samples doped with increasing CoO amounts: 1.5 wt.%, 2 wt.%, and 3 wt.% and those co-doped with CoO and Cu_2O of some different amount are presented in Fig. 1(b). No peaks corresponding to a second phase are detected for any of the samples, even for the sample highly doped with CoO 3 wt.% + Cu_2O 1 wt.%. This suggests that the cations of the additives diffuse into the mother

phase without undergoing the reaction that forms a second phase. Alternatively, they diffuse and remain at the grain boundary region without forming sufficient volume of the second crystalline phase required to be detectable via XRD.

Figures 2(a)–2(f) show the SEM micrographs of the NZF samples doped with 1 wt.% of the different types of additives sintered at 1250 °C. A highly dense microstructure is commonly revealed for all the samples, but the grain shapes and sizes slightly differ with the type of additive. The density and average grain size (D_{ave}) of these samples are presented in Table 1. The doped samples

have a slightly higher density than the undoped NZF sample. The samples doped with CoO (Fig. 2(b)) show a similar microstructure to that of the undoped sample (Fig. 2(a)) with a similar D_{ave} of ~1.7 μm. It is found that the grain growth in the samples doped either with SiO$_2$ (Figs. 2(d)) or MgO (Figs. 2(f)) is prohibited by these additives and the sample D_{ave} is relatively smaller than that of the undoped NZF. Contrastingly, doping by Cu$_2$O (Fig. 2(c)) or CaCO$_3$ (Fig. 2(e)) promotes grain growth, and these samples have a larger D_{ave} than the undoped sample. It is also noted that increasing the CoO doping amount up to 3 wt.% does not have a significant effect on the microstructure of the samples. Note that the 1.5-3 wt.% CoO-doped samples shows a similar microstructure with D_{ave} in the range of 1.6-1.8 μm (Figs. 2(g), 2(h), and 2(i)). In case of 1.5 wt.% CoO and 0.5 wt.% Cu$_2$O co-doping, D_{ave} increases to 2.31 μm (Fig. 2(j)). Abnormally grown very large grains are found in the samples co-doped with CoO–Cu$_2$O (1 wt.%). The D_{ave} of these two samples, as shown in Fig. 2(k) and 2(l), is larger than ~10 μm. Co-doping the sample with CoO and 1 wt.% of Cu$_2$O causes a very large grain growth. However, individual doping with 1-3 wt.% CoO and 1 wt.% Cu$_2$O (Fig. 2(c)), respectively, leads to a normal grain growth and does not cause a significant microstructure change. It is very interesting to note that there is some mutual interplay between the sintering additives, Cu$_2$O and CoO, for the enhanced grain growth of the ceramics.

The B–H hysteresis curves of the NZF samples are presented in Figs. 3(a)-3(d). Typical Ni–Zn spinel ferrites are soft magnetic materials having an intrinsic coercivity (H_C) value less than a few Oersteds. Here, the B–H measurements were conducted by using the toroidal B–H measurement technique [17]. The demagnetizing field effect is completely avoided in the toroidal sample geometry because no magnetic poles are present in the sample. The measured H_C and magnetic flux density at H = 30 Oe ($B_{H=30Oe}$) are collected and presented in Table 1. The undoped NZF0 sample has H_C = 0.33 Oe and $B_{H=30Oe}$ = 3755 G. Among the samples doped with 1 wt.% CoO, Cu$_2$O, SiO$_2$, CaCO$_3$, and MgO, respectively, only the Cu$_2$O-doped sample has a smaller H_C of 0.26 Oe than the NZF0 sample. This is owing to the larger grain size of this sample (D_{ave} = 2.24 μm). Previous studies [18-21] have reported that the H_C decrease with increasing grain size, where the grain size is on the micrometer scale, follows the equation:

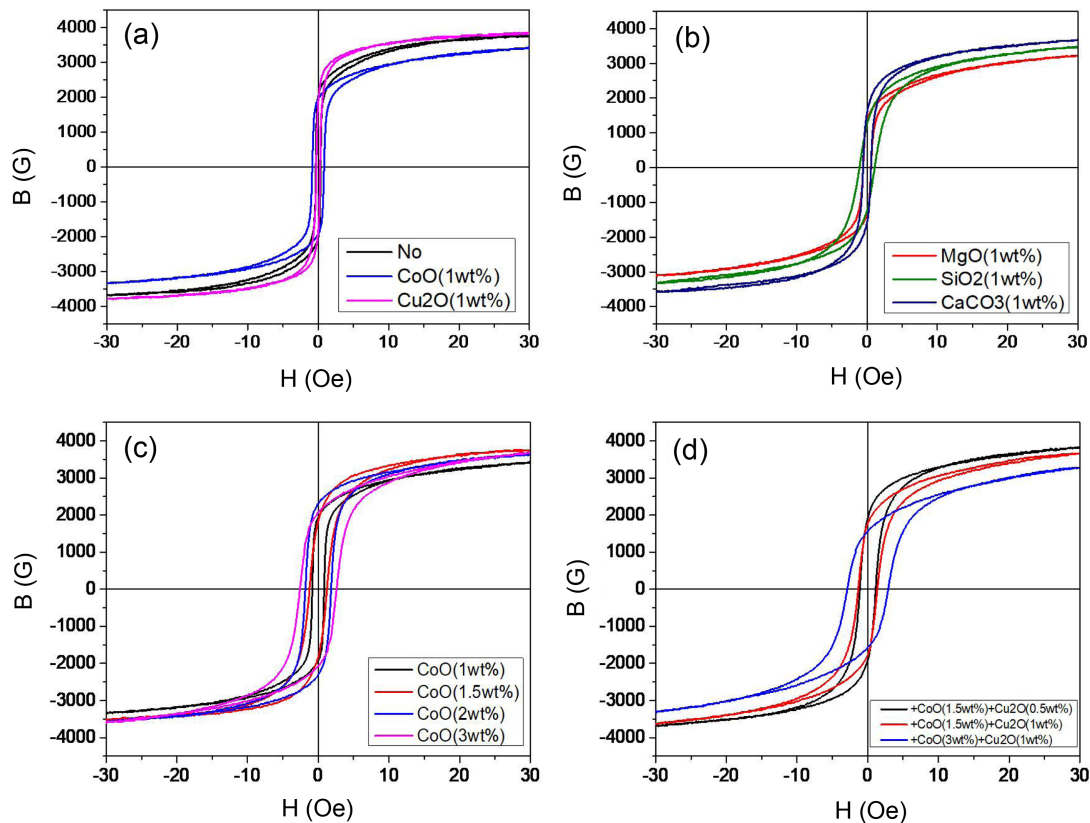$$H_C = C_1 \frac{\sqrt{AK_1}}{D \cdot M_S} \qquad (1)$$

Fig. 3. (Color online) (a)–(d) B–H hysteresis curves of Ni$_{0.4}$Zn$_{0.6}$Fe$_2$O$_4$ ferrite with various additives.

where C_1 is a constant, A is the exchange stiffness, K_1 is the crystalline anisotropy constant, D is the grain size, and M_S is the saturation magnetization. The reciprocal relationship between H_C and D is related to the domain wall pinning at the grain boundaries. However, the CaCO$_3$-doped sample has a larger H_C value (0.56 Oe) than the NZF0 sample even though it has a larger grain size. This is possibly attributed to the additional domain wall pinning by the impurities of Ca-compound that exist at the grain boundaries because substitution of large Ca ions in the cation sites of the Ni–Zn ferrite phase cannot be expected. Among the samples with various additives of 1

wt.%, the maximum H_C of 1.08 Oe is obtained for the SiO$_2$-doped sample (NZF3) because SiO$_2$ suppresses the grain growth most effectively. As the doping amount of CoO is increased up to 3 wt.%, H_C of the samples increases gradually without a change in the micro-structure. In this case, the increase in H_C is attributable to intrinsic effects such as increase in the crystalline anisotropy (K_1) of the spinel phase. This is an indirect evidence that Co ions are substituted in the crystal lattice of the spinel structure. Even the maximum H_C value of 2.9 Oe is obtained in the CoO (3 wt.%) + Cu$_2$O (1 wt.%)-doped sample (NZF11), which shows an abnormal grain growth
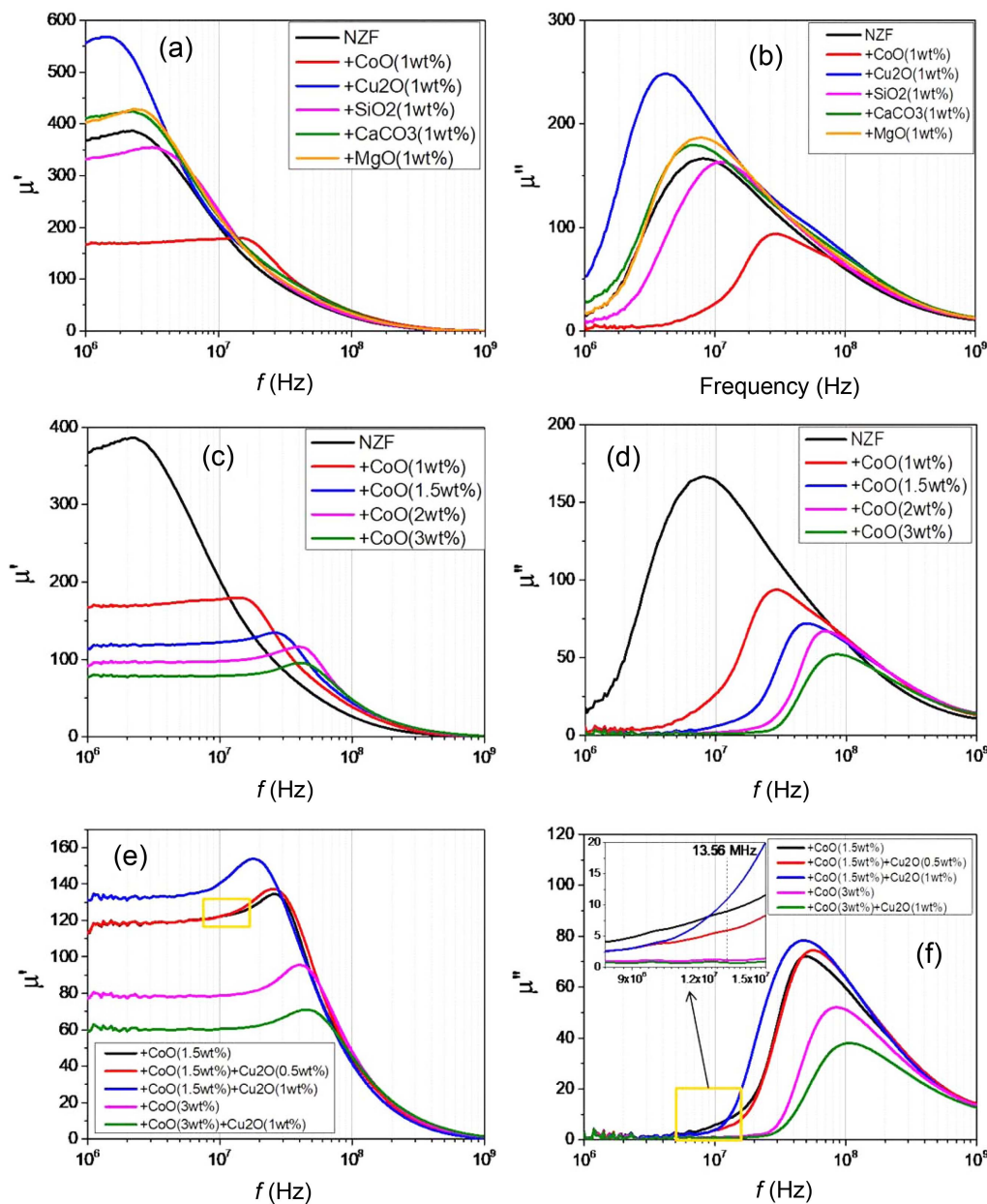
Fig. 4. (Color online) (a)–(f) Frequency-dependent real (μ') and imaginary (μ'') parts of the permeability of Ni$_{0.4}$Zn$_{0.6}$Fe$_2$O$_4$ ferrite with various additives.

(D$_{ave}$ > 10 μm). The B$_{H=30}$ value also varies with the additives. However, these values are not very relevant because magnetic field H = 30 Oe is not sufficient for achieving magnetic saturation. A sample with a higher H_C exhibits a slower magnetization behavior, and thus, it has a lower B$_{H=30}$ value. Based on our previous research, the NZF0 sample has a saturation magnetization (M_S) of 62.3 emu/g [15], corresponding to $4\pi M_S$ = 4116 G.

Figures 4(a)-4(f) show the frequency-dependent complex permeability of the NZF samples. Relevant parameters, such as the real part of the permeability (μ') at 1 MHz, maximum imaginary part of the permeability (μ''_{max}), and frequency at the maximum μ'' (f$_{\mu''max}$), obtained from the curves are also presented in Table 1. Practically in this research, the real part of the permeability at 1 MHz can be defined as static permeability μ_s'. In Figs. 4(a) and 4(b), it is found that doping with SiO$_2$ and CoO shifts the spectra of μ' and μ'' to a higher frequency as the height of the spectra decreases, whereas doping with the other additives shifts them in the opposite direction. In case of the Cu$_2$O-doped NZF sample having a larger D$_{ave}$ and smaller H$_C$ than the undoped NZF, both the μ', μ'' spectra shift to the left side with a higher static permeability (μ_s') and higher peak in the μ'' spectra. SiO$_2$ doping that causes a finer grain structure and larger H$_C$ than without doping, makes the μ', μ'' spectra to shift to the right direction. Among the various additives (1 wt.%), CoO and Cu$_2$O are effective in modulating the μ', μ'' spectra because CoO shifts the spectra to the right direction, whereas Cu$_2$O shifts it to the left direction more largely than the other additives. The high-frequency complex permeability (μ', μ'') spectra are obtained from the contribution of both the domain wall vibration and spin motions. Thus, they are related to both the extrinsic and intrinsic factors of the materials. The domain wall contribution to the permeability is more dominated by extrinsic factors such as the grain size (D), whereas the spin contribution portion is more closely related to intrinsic factors such as the crystalline anisotropy (K_1). The relationship between initial permeability μ_i and the above-mentioned material parameters is given by the equation following [18]:

$$\mu_i = C_2 \frac{D \cdot M_S^2}{\sqrt{A K_1}} \tag{2}$$

On increasing the CoO addition up to 3 wt.%, both the μ', μ'' spectra gradually shift to a higher frequency following Snoek's law, as shown in Figs. 4(c) and 4(d). This gradual spectrum shift is owing to the increase in the magnetocrystalline anisotropy caused by the gradual substitution of Co in the spinel ferrite lattices. Note that the SEM images of the CoO-doped NZF samples, presented

in Figs. 2(g)-2(i), show similar microstructures and D$_{ave}$ in the samples.

The co-doping effect of the two effective additives, CoO and Cu$_2$O, on the permeability spectra was also investigated. When the f$_{\mu''max}$ values of the samples in Table 1 are compared with each other, it is understandable that the Co doping amount is a dominant factor in shifting the μ', μ'' spectra. Although there is a large difference in the grain size between the two samples of NZF6 (CoO 1.5 wt.%) and NZF10 (CoO 1.5 wt.% + Cu$_2$O 1 wt.%), the f$_{\mu''max}$ values are very close (49.6 and 47.9 for NZF6 and NZF10, respectively). This is because the spin contribution to the μ', μ'' spectra of NZF is more dominant than the domain contribution and the intrinsic factor K_1 can be tuned by the Co doping amount. Still, the co-doping of Cu$_2$O with CoO gives a significant effect on tuning the μ' and μ'' profile delicately. In Figs. 4(e) and 4(f), the spectra of the NZF samples co-doped with CoO and Cu$_2$O are compared to those of 1.5 wt.% and 3 wt.% CoO individually doped NZF samples. The combination of CoO 1.5 wt.% + Cu$_2$O 0.5 wt.% effectively depresses the magnetic loss related factor of μ'' without decreasing μ' near 10 MHz. The NZF sample co-doped with 1.5 wt.% CoO + 0.5 wt.% Cu$_2$O simultaneously exhibits a smaller μ'' (5.8) and larger μ' (125.3) than 1.5 wt.% CoO individually doped NZF (μ' = 124.0, μ'' = 5.9) at the frequency of 13.56 MHz.

4. Conclusions

Highly dense Ni$_{0.4}$Zn$_{0.6}$Fe$_2$O$_4$ samples (toroidal-type) were successfully prepared by conventional ceramic processes with various additives, namely, CoO, Cu$_2$O, SiO$_2$, CaCO$_3$, MgO, and combinations of CoO and Cu$_2$O. The complex permeability (μ', μ'') spectra could be effectively modulated by the additives of Cu$_2$O and CoO. The CoO doping shifted the μ', μ'' spectra to a higher frequency (f), whereas Cu$_2$O shifted the spectra to a lower f. The sample co-doped with 1.5 wt.% CoO and 0.5 wt.% Cu$_2$O had a slightly larger μ' (125.3) with a smaller μ'' (5.9) than the 1.5 wt.% CoO individually doped sample (μ' = 124.0, μ'' = 9.0) at the frequency of 13.56 MHz. The above result is very promising for RFID magnetic field shielding or low-loss inductor core applications.

Acknowledgments

References

[1] A. Goldman, Handbook of Modern Ferromagnetic Materials, Kulwer Academic Publishers, Boston (1999).

[2] T. Tsutaoka, J. Appl. Phys. **93**, 2789 (2003).

[3] S.-S. Kim, D.-H. Han, and S.-B. Cho, IEEE Trans. Magn. **30**, 4554 (1994).

[4] S. T. Mahmud, A. K. M. Akther Hossain, A. K. M. Abdul Hakim, M. Seki, T. Kawai, and H. Tabata, J. Magn. Magn. Mater. **305**, 269 (2006).

[5] N. N. Jiang, Y. Yang, Y. Zhang, J. Zhou, and P. Liu, J. Magn. Magn. Mater. **401**, 370 (2016).

[6] I. H. Gul, W. Ahmed, and A. Maqsood, J. Magn. Magn. Mater. **320**, 270 (2008).

[7] M. M. Rashad, E. M. Elsayed, M. M. Moharam, R. M. Abou-Shahba, and A. E. Saba, J. Alloy. Compd. **486**, 759 (2009).

[8] S. Zahi, M. Hashim, and A. R. Daud, J. Magn. Magn. Mater. **308**, 177 (2007).

[9] S. E. Shrsath, B. G. Toksha, R. H. Kadam, S. M. Patange, D. R. Mane, G. S. Jangam, and A. Ghasemi, J. Phys. Chem. Sol. **71**, 1669 (2010).

[10] T. Nakamura, J. Appl. Phys. **88**, 348 (2000).

[11] T. Tsutaoka, J. Appl. Phys. **93**, 2789 (2003).

[12] I. H. Gul, W. Ahmed, and A. Maqsood, J. Magn. Magn. Mater. **320**, 270 (2008).

[13] M. S. Ruiz, P. G. Bercoff, and S. E. Jacobo, Ceram. Inter. **39**, 4777 (2013).

[14] N.-N. Jiang, Y. Yang, Y.-X. Zhang, J.-P. Zhou, P. Liu, and C.-Y. Deng, J. Magn. Magn. Mater. **401**, 370 (2016).

[15] K.-R. Mun and Y.-M. Kang, J. Korean Magn. Soc. **28**, 93 (2018).

[16] A. Hajalilou, M. Hashim, R. Ebrahimi-Kahrizsangi, and N. Sarami, J. Phys. D: Appl. Phys. **48**, 145001 (2015).

[17] J. C. Mallinson, The foundations of magnetic recording, 2nd edition, Academic Press Ltd., London (1993) pp 13-14.

[18] G. Herzer, IEEE Trans. Magn. **26**, 1397 (1990).

[19] M. M. Syazwan, A. N. Hapishah, R. S. Azis, Z. Abbas, and M. N. Hamidon, Results Phys. **9**, 842 (2018).

[20] J.-E. Yoo, T. W. Hong, and Y.-M. Kang, J. Korean Magn. Soc. **28**, 219 (2018).

[21] E.-S. Lim, Y.-M. Kang, and D.-Y. Kim, J. Korean Magn. Soc. **29**, 1 (2019).